Statistical modeling of a former Arctic Ocean ice shelf complex using Antarctic analogies

Furrer, Reinhard ; Jakobsson, Martin ; Kirchner, Nina ; Robbins, John W ; Zwally, H Jay

Abstract: Geophysical mapping and coring of the central Arctic Ocean seafloor provide evidence for repeated occurrences of ice sheet/ice shelf complexes during previous glacial periods. Several ridges and bathymetric highs shallower than present water depths of 1000m show signs of erosion from deep-drafting (armadas of) icebergs, which originated from thick outlet glaciers and ice shelves. Mapped glacigenic landforms and dates of cored sediments suggest that the largest ice shelf complex was confined to the Amerasian sector of the Arctic Ocean during Marine Isotope Stage (MIS) 6. However, the spatial extent of ice shelves can not be well reconstructed from occasional groundings on bathymetric highs. Therefore, we apply a statistical approach to provide independent support for an extensive MIS 6 ice shelf complex, which previously was inferred only from interpretation of geophysical and geological data. Specifically, we assess whether this ice shelf complex comprises a likely source of the deep-draft icebergs responsible for the mapped scour marks. The statistical modeling is based on exploiting relations between contemporary Antarctic ice shelves and their local physical environments and the assumption that Arctic Ocean MIS6 ice shelves scale similarly. Analyzing ice thickness data along the calving front of contemporary ice shelves, a peak over threshold method is applied to determine sources of deep-drafting icebergs in the Arctic Ocean MIS6 ice shelf complex. This approach is novel to modeling Arctic paleoglacial configurations. Predicted extreme calving front drafts match observed deep-draft iceberg scours if the ice shelf complex is sufficiently large. Key Points Arctic Ocean deep-draft ice berg scours supported by statistical modeling Novel application of Extreme Value Theory in modeling paleoglacial systems Analogies between present Antarctic/fomer Arctic ice shelf configurations.

DOI: https://doi.org/10.1002/jgrf.20077

JOURNAL OF GEOPHYSICAL RESEARCH: EARTH SURFACE, VOL. 118, 1105–1117, doi:10.1002/jgrf.20077, 2013

Statistical modeling of a former Arctic Ocean ice shelf complex using Antarctic analogies

N. Kirchner,[1] R. Furrer,[2] M. Jakobsson,[3] H. J. Zwally,[4] and J. W. Robbins[4]

Received 13 March 2012; revised 29 March 2013; accepted 23 April 2013; published 18 June 2013.

[1] Geophysical mapping and coring of the central Arctic Ocean seafloor provide evidence for repeated occurrences of ice sheet/ice shelf complexes during previous glacial periods. Several ridges and bathymetric highs shallower than present water depths of ∼ 1000 m show signs of erosion from deep-drafting (armadas of) icebergs, which originated from thick outlet glaciers and ice shelves. Mapped glacigenic landforms and dates of cored sediments suggest that the largest ice shelf complex was confined to the Amerasian sector of the Arctic Ocean during Marine Isotope Stage (MIS) 6. However, the spatial extent of ice shelves can not be well reconstructed from occasional groundings on bathymetric highs. Therefore, we apply a statistical approach to provide independent support for an extensive MIS 6 ice shelf complex, which previously was inferred only from interpretation of geophysical and geological data. Specifically, we assess whether this ice shelf complex comprises a likely source of the deep-draft icebergs responsible for the mapped scour marks. The statistical modeling is based on exploiting relations between contemporary Antarctic ice shelves and their local physical environments and the assumption that Arctic Ocean MIS 6 ice shelves scale similarly. Analyzing ice thickness data along the calving front of contemporary ice shelves, a peak over threshold method is applied to determine sources of deep-drafting icebergs in the Arctic Ocean MIS 6 ice shelf complex. This approach is novel to modeling Arctic paleoglacial configurations. Predicted extreme calving front drafts match observed deep-draft iceberg scours if the ice shelf complex is sufficiently large.

Citation: Kirchner, N., R. Furrer, M. Jakobsson, H. J. Zwally, and J. W. Robbins (2013), Statistical modeling of a former Arctic Ocean ice shelf complex using Antarctic analogies, *J. Geophys. Res. Earth Surf.*, *118*, 1105–1117, doi:10.1002/jgrf.20077.

1. Introduction

[2] Hypotheses on glacial conditions in the Arctic Ocean range from the suggestion of total absence of sea ice [*Ewing and Donn*, 1956] to existence of a coherent, thick ice shelf covering the entire Arctic Ocean [*Mercer*, 1970; *Broecker*, 1975; *Hughes et al.*, 1977]. These hypotheses were put forward long before icebreakers and nuclear submarines were able to reach the pack-ice covered central Arctic Ocean and map the seafloor. Over the last decade, geophysical mapping of the Arctic seafloor has revealed extensive erosion caused by ice and glacial landforms on ridge crests and plateaus where present water depths are shallower than ∼1000 m [*Jakobsson*, 1999; *Polyak et al.*, 2001].

[3] Yet not all bathymetric highs shallower than 1000 m contain signs of ice impact. Instead, the accumulated geological and geophysical data suggest more limited ice shelves with the most extensive ones constrained to the Amerasian Basin during Marine Isotope Stage (MIS) 6 (Figure 1) [*Jakobsson et al*., 2010]. In this basin, smaller ice shelves likely also existed during later glacial periods, including the Last Glacial Maximum [*England et al.*, 2009; *Polyak and Jakobsson*, 2011]. The extent of an ice shelf cannot be reconstructed by geophysical mapping alone, because ice shelves when floating leave no distinct marks behind on the seafloor, in contrast to grounded ice sheets and fast-flowing ice streams. Therefore, spatial reconstructions of the extents of these Amerasian Arctic Ocean ice shelves are necessarily based on indirect evidence (Figure 1) while spatial reconstructions of paleo ice sheets may be based on diagnostic landforms outlining their maximum extents [*Kleman et al.*, 2006].

[4] The widely-used numerical shallow ice approximation ice sheet models do not properly simulate ice streams and coupled ice shelves [*van der Veen et al.*, 2007; *Hindmarsh*, 2009; *Kirchner et al.*, 2011]. Ongoing

Additional supporting information may be found in the online version of this article.

[1]Department of Physical Geography and Quaternary Geology, Stockholm University, Stockholm, Sweden.
[2]Institute of Mathematics, University of Zurich, Zurich, Switzerland.
[3]Department of Geological Sciences, Stockholm University, Stockholm, Sweden.
[4]Cryospheric Sciences Branch, NASA Goddard Space Flight Center, Greenbelt, Maryland, USA.

Corresponding author: N. Kirchner, Department of Physical Geography and Quaternary Geology, Stockholm University, 106 91 Stockholm, Sweden. (nina.kirchner@natgeo.su.se)

2169-9003/13/10.1002/jgrf.20077

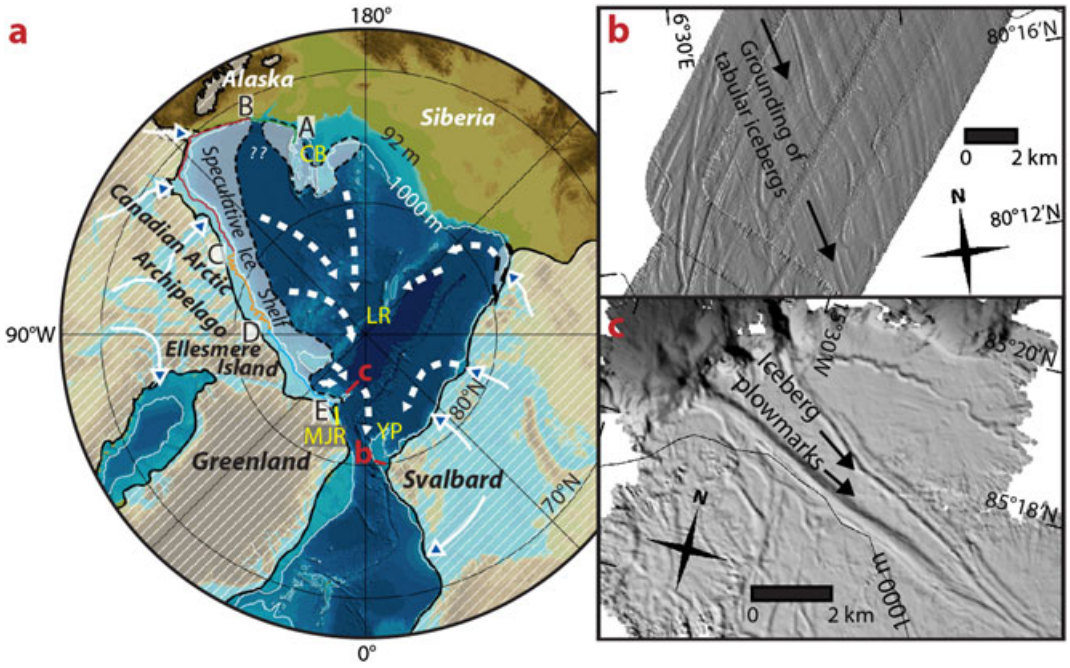

Figure 1. (a) The hypothesized extension of an ice shelf complex in the Amerasian Arctic Ocean during MIS 6. The map is modified from *Jakobsson et al.* [2010]. The grounding line of the MIS 6 ice shelf complex is assumed to follow the present continental shelf break and is divided into individual segments A–B, B–C, C–D, and D–E used in the statistical modeling. Abbreviations are: MJR, Moris Jesup Rise; YP, Yermak Plateau; LR, Lomonosov Ridge; CB, Chukchi Borderland. (b) Multibeam mapped glacigenic features on the Yermak Plateau extending from the northern Svalbard continental margin (location shown in Figure 1a). These features, resembling mega-scale glacial lineations, were interpreted by *Jakobsson et al.* [2010] and *Dowdeswell et al.* [2010] to be formed from grounding of tabular icebergs on their way to exit the Arctic Ocean through the Fram Strait. (c) Iceberg scours on the Morris Jesup Rise, north of Greenland. These iceberg scours are located deeper than 1000 m present water depth, and sediment draped atop suggests that they were formed during MIS 6 [*Jakobsson et al*., 2010].

modeling efforts focusing on advanced marginal ice dynamics, ice sheet-ice shelf coupling, and disintegration of ice shelves aim to provide improved prognostic centennial-scale simulations in time for the 5th Assessment Report of the IPCC (cf. the community projects Ice2sea and SeaRise, http://www.ice2sea.eu, http://websrv.cs.umt.edu/isis/index.php/SeaRISE-Assessment). Numerical simulations for ice shelf complexes during glacial cycles are rare. Early experiments with focus on the Arctic employed simplified representations of sheet-shelf dynamics [*Siegert and Dowdeswell*, 1999; *Siegert et al.*, 2001], while more recent simulations account for complex dynamics but have not yet been applied exclusively to Arctic Ocean ice shelves [*Pattyn*, 2003; *DeConto et al.*, 2007; *Peyaud et al.*, 2007; *Pollard and DeConto*, 2009; *Alvarez-Solas et al.*, 2011; *Fyke et al.*, 2011].

[5] Here we propose a new modeling framework with the aim to amend the spatial reconstruction of the MIS 6 Arctic Ocean ice shelf complex presented by *Jakobsson et al.* [2010] with an assessment of whether this proposed large Arctic Ocean ice shelf complex can also be supported on statistical grounds. Using appropriate statistical modeling, we specifically address the question of whether the suggested MIS 6 Amerasian ice shelf complex comprised a likely source for the deep-drafting icebergs that grounded in the central Arctic Ocean and of which there is mapped evidence.

[6] The statistical approach adopted here is based on establishing functional relations between key characteristics determining the configurations of current Antarctic ice shelves. Assuming that similar relations held for the Amerasian ice shelves during MIS 6, we predict selected features of this ice shelf complex. Specifically, we derive quantitative estimates of ice shelf area, calving front length and the maximal draft (depth below sea level) along the calving front. We emphasize that we do not claim present-day Antarctic conditions to represent a perfect analog for former glacial conditions in the Arctic Ocean. Nonetheless, our modeling approach provides a range of possible Arctic Ocean paleo ice shelf configurations, based on considering present dimensions and conditions of Antarctic ice shelves as well as firmly based statistical techniques. By construction, our analysis is limited to modeling static ice shelf configurations at arbitrary model times only. Therefore, it is applicable to any other ice shelf system of the Quaternary glacial periods, of which the here investigated MIS 6 Amerasian ice shelf complex in the Arctic Ocean is but one example. In particular, we do attempt neither to prove the ice shelf complex's existence nor to perform a realistic paleo simulation comparable to those performed with

Table 1. Contemporary Antarctic Ice Shelves Used in the Statistical Analysis[a]

Variable	Notation
Length of calving front[b]	y_{len}
Total ice shelf area (with rises)[b]	y_{area}
Draft along calving front	y_{draft}
Length of grounding line[b]	x_{ground}
Max. ice thickness at grounding line[b]	x_{thick}
Number of ice rises	x_{rise}
Ice shelf geometry	x_{geom}
Water temperature at calving front	x_{temp}

[a]Contemporary Antarctic ice shelves used in the analysis, and eight data variables and their abbreviations, as well as the classification of the variables into responses (y), predictors (x), and draft (y_{draft}) are indicated as follows: Abbot* ("open"), Amery ("embayed"), Brunt (open), Dotson* (embayed), Drygalski (open), Ekström (embayed), Filchner (embayed), Fimbul (open), Getz* (open), Mertz Glacier (open), Ninnis Glacier* (embayed), Pine Island Glacier* (embayed), Riiser–Larsen (open), Ronne (embayed), Ross (embayed), Shackleton (open), West (open). x_{geom} has binary values only (open/embayed) and is therefore listed in parentheses after each ice shelf name in the list of the 17 ice shelves considered. For the five starred ice shelves, the maximal draft values at their respective calving fronts are not considered in the EVT since they are considered to be not representative, see section 2.1 and Figure S6 of the supporting information. Water temperatures are derived from the WOCE database [*Orsi and Whitworth*, 2004], all other variables are based on *Bohlander and Scambos'* [2007] MODIS data and *DiMarzio et al.'s* [2007] ICESat data, the latter in combination with the algorithm of *Zwally et al.* [2005] to compute ice shelf thickness. Details on the processing of the data are given in the supporting information.

[b]The original data has been log-transformed (natural logarithm). For notational simplicity, we omit the log notation in the text as, from the context, it is clear whether we use the original or transformed scale.

thermodynamically coupled, continuum-mechanics based coupled ice sheet models.

2. Statistical Modeling Framework: Data and Methodology

[7] We focus on the MIS 6 ice shelf complex put forward as a hypothesis by *Jakobsson et al.* [2010]. Fed by ice streaming in major bathymetric troughs of the Canadian Arctic Archipelago, this complex is reconstructed as several merged ice shelves extending into the Arctic Ocean from the continental shelf between north of Alaska in the west and northern Greenland in the east. This reconstruction represents a generalized view of the maximum MIS 6 marine ice sheet extension. It is based on sediment coring and geophysical mapping that revealed iceberg plowmarks and features resembling mega-scale glacial lineations on bathymetric highs (Morris Jesup Rise, Yermak Plateau, Lomonosov Ridge, and Chukchi Borderland) as deep as $\sim$1000 m below present sea level (Figure 1).

[8] Using statistical modeling, we address the question whether the suggested MIS 6 Amerasian ice shelf complex comprised a likely source for the deep-drafting icebergs that grounded in the central Arctic Ocean. This requires modeling of draft values along the calving front of the ice shelf complex. Because no direct evidence exists that outline its spatial extent, we also include modeling of its total area and calving front length. Moreover, since there are no analog ice shelves in the Arctic Ocean today, the statistical modeling is based on relations between characteristic variables for present Antarctic ice shelves and their local physical environments. Once these relations are established, the model is applied to the paleo-Arctic setting. The following three-step methodology is applied (and detailed in the following sections):

[9] 1. Establish statistical relations between characteristic variables for contemporary Antarctic ice shelves through fitting of a multivariate linear model (MLM), cf. section 2.2.

[10] 2. Model the largest drafts along the calving front of contemporary Antarctic ice shelves using extreme value theory (EVT), more specifically, apply a peak over threshold (POT) approach to model exceedances of draft above a high, preselected threshold, cf. section 2.3.

[11] 3. Predict Arctic Ocean MIS 6 calving front length, maximal draft along the calving front, and ice shelf area by application of the model derived in steps 1 and 2, cf. section 3.

[12] In step 1, Antarctic data is used to fit a MLM composed of two regressions with several predictors and correlated errors between both responses. Seventeen Antarctic ice shelves are included, each characterized by eight variables. The latter are classified as "predictors" (x) or "responses" (y), with corresponding subscripts (Tables 1, 2) .

[13] In step 2, draft along the calving front, y_{draft}, is extracted as a sequence of observations for each shelf from the Antarctic data set (Table 1). We are interested in extremely large or even the largest drafts and, hence, employ EVT to predict which draft value is exceeded on average at least once along the calving front. We refer to this value as the "return draft"; the concept is borrowed from models of hydrological events in which "return level" and "return period" are used to describe "100 year-floods," i.e., the return level that has 1% chance of being exceeded in a given year [*Coles*, 2001; *Katz et al.*, 2002]. In our case, the return period is associated with length of calving front instead of time. Thus, the m-kilometer return draft is expected to be exceeded on average once every m kilometers along the calving front. Note that, for five ice shelves out of the considered 17, the available y_{draft} data could not be used in the EVT, reducing thus the number of ice shelves

Table 2. Averaged Water Temperature x_{temp} (in °C) at the Calving Front[a]

Ice Shelf	x_{temp}	Stations Considered	Draft Range $[\Delta_{\min}, \Delta_{\max}]$, in Meters Below Sea Level
Abbot	–1.77	2	[50,110]
Amery	–1.72	30	[100,200]
Brunt	–1.75	23	[50,100]
Dotson	–1.63	4	[75,150]
Drygalski	–1.83	23	[50,110]
Ekström	–1.86	16	[90,160]
Filchner	–2.01	50	[250,450]
Fimbul	–1.77	22	[100,250]
Getz	–1.49	9	[125,200]
Mertz	–1.58	15	[75,175]
Ninnis	–1.77	9	[80,150]
Pine Island	–1.04	3	[125,250]
Riiser-Larsen	–1.61	125	[100,180]
Ronne	–1.88	103	[200,450]
Ross	–1.73	243	[200,300]
Shackleton	–1.29	26	[175,275]
West	–1.63	32	[100,250]

[a]Extracted and post-processed from [*Orsi and Whitworth*, 2004] to fit the interval $[\Delta_{\min}, \Delta_{\max}]$, see also the supporting information.

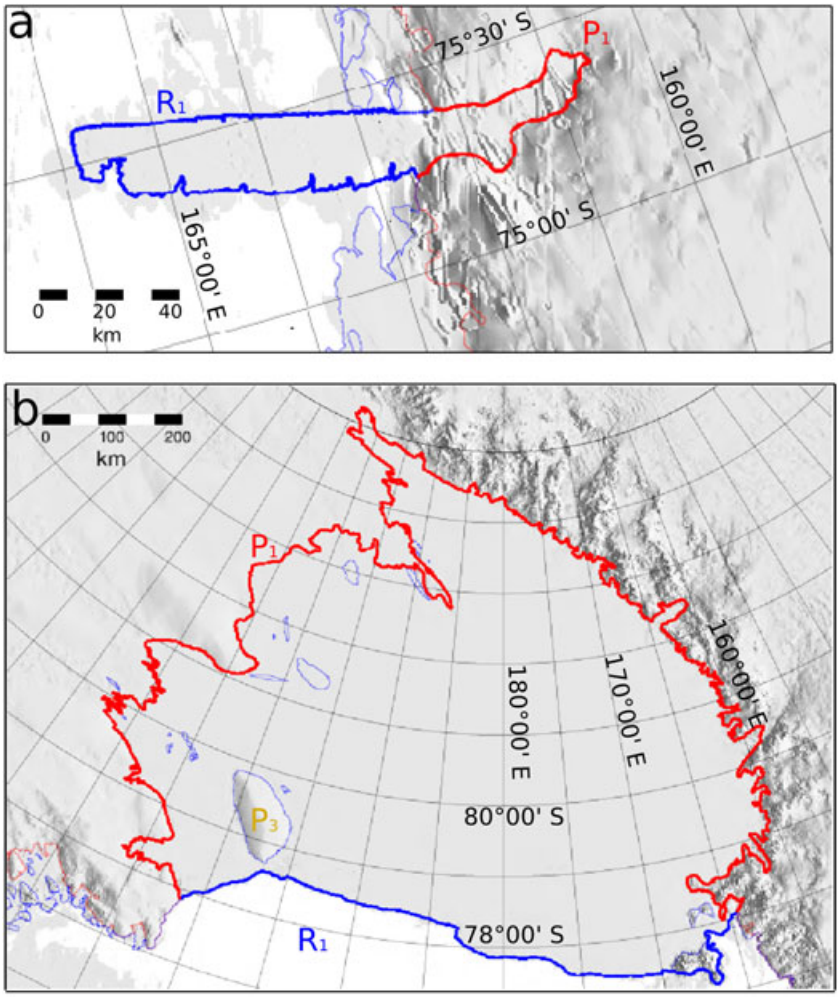

Figure 2. Examples of ice shelves of geometry "open" and "embayed" (predictor x_{geom}). Grounding line (red, length depicting predictor x_{ground}), calving front (blue, y_{len}), and contours of ice rises (the total number of which constitutes x_{rise}) are based on *Bohlander and Scambos'* [2007] MODIS Mosaic of Antarctica (MOA). (a) Drygalski ice tongue (open), (b) Ross ice shelf (embayed). Note the different scales in both panels.

considered in this step to 12, cf. also the supporting information, Appendix SA.

[14] In step 3, the statistical model derived in step 1 and 2 is applied to predict calving front length, ice shelf area, and a probabilistic description of the maximum draft along the calving front of the Arctic Ocean MIS 6 ice shelf complex. This is expected to help identify likely source regions for icebergs large enough to scour the seafloor at ∼1000 m below sea level. The results also indicate the range of possible ice shelf configurations, of which one is suggested in *Jakobsson et al.* [2010]. Paleo ice shelf variables corresponding to Antarctic predictors are required as input.

2.1. Ice Shelf Data

2.1.1. Contemporary Antarctic Data

[15] Contemporary Antarctic ice shelf data (y_{len}, y_{area}, y_{draft}, x_{ground}, x_{thick}, and x_{rise}, see Table 1) are derived from *Bohlander and Scambos'* [2007] MODIS Mosaic of Antarctica, in combination with *DiMarzio et al.'s* [2007] digital elevation model (DEM) obtained from the first seven observation campaigns of the Geoscience Laser Altimeter System instrument (2003–2005) aboard ICESat and *Zwally et al.'s* [2005] algorithm to compute ice shelf thickness. Elevations in the DEM refer to the EGM96 geoid. Length of calving front, y_{len} and length of grounding line, x_{ground} are defined such that their sum equals the total length of the ice shelf boundary (Figure 2).

[16] Furthermore, we have introduced a binary variable, x_{geom}, to classify the shape of an ice shelf as either open or embayed. Specifically, we let the ratio $c := y_{len}/x_{ground}$ determine ice shelves with $c \geq 1$ as open, and ice shelves with $c < 1$ as embayed. This geometric criterion may coincide with the intuitive notion of an embayed ice shelf, but does not by necessity. For instance, Abbot ice shelf, Riiser-Larsen ice shelf and Shackleton ice shelf are classified as open, for reasons explained in the supporting information.

[17] Water temperatures x_{temp} are retrieved from the World Ocean Circulation Experiment Southern Ocean Data Base [*Orsi and Whitworth*, 2004], cf. Table 2. A more

Table 3. Length of Individual Paleo-Grounding Line Segments in the Amerasian Basin of the Arctic Ocean, and Combinations Thereof [a]

Segment	Length of Grounding Line x_{ground}	Number of Ice Rises x_{rise}	Ice Shelf Geometry x_{geom}
A–B	1746 km	2	—
B–C	5310 km	0	embayed
C–D	3606 km	0	open
D–E	2862 km	2	open
A–C	7056 km	2	embayed
A–E-e	13524 km	4	embayed
A–E-o	13524 km	4	open
B–E	11778 km	2	open

[a]Four different uniform (that is, identical along all ice shelf fronts) water temperatures x_{temp} are considered (0, –1, –1.8 and –2° C). Segment A–B has not been classified individually as it is only considered in combination with other segments.

detailed description of the data is provided in the supporting information, Appendix SA.

[18] Note that the statistical modeling framework does not limit the number of ice shelves or variables considered but the types of variables. Specifically, we have neither included Antarctic Peninsula ice shelves in our analysis, nor have we accounted for any spatially variable data fields other than y_{draft} and x_{temp}, respectively; we provide justification for these restrictions in section 4.

2.1.2. Paleo-Arctic Data

[19] The paleo ice shelf predictors x_{ground}, x_{rise} and x_{geom} are derived under the assumption that the Laurentide ice sheet reached the continental shelf break and from there extended as an ice shelf. Hence, the present location of the shelf break is taken as the grounding line position of the MIS 6 ice shelf. Using the International Bathymetric Chart of the Arctic Ocean (IBCAO) gridded bathymetric model Version 2.0 [*Jakobsson et al.*, 2008a], the shelf break/grounding line is digitized. This clearly implies a maximum scenario for the MIS 6 ice sheet extension. The physiographic setting and locations of feeding ice streams, inferred from glacial troughs distinguished in the bathymetry, suggest a subdivision of the grounding line of the ice shelf complex into four segments: A–B, B–C, C–D, and D–E (Figure 1). The segment length is used as input data (x_{ground}) for the statistical modeling (Table 3). Note that a meaningful comparison of lengths of paleo and contemporary grounding lines has to compensate for possible differences in measuring resolution (cf. the supporting information, Appendix SB and Figure S2 for details). To prescribe the paleo-predictors x_{rise} and x_{geom} from inspection of IBCAO, a sea level 92 m below the present is assumed for MIS 6 [*Rabineau et al.*, 2006]. The response of the ice shelf complex to different water temperatures, x_{temp}, along the calving front is investigated. Maximum ice thickness at grounding line, x_{thick}, is not required during model application to the paleo-Arctic.

2.2. Multivariate Linear Model (MLM)

[20] Contemporary Antarctic ice shelf data forms the basis of our MLM. Using common statistical practice, we evaluate if responses or predictors need to be transformed to establish functional relations between Antarctic predictors and responses. The responses as well as some predictors have been log-transformed (natural logarithm; see Table 1), but for simplicity we omit the log notation. Note that we do not claim any causality between the predictors and responses as is usually done in classical regression analysis. The intuitive dependence between length of ice shelf calving front y_{len} and total ice shelf area y_{area} is confirmed (using Pearson's correlation coefficient as a criterion) and suggests a modeling approach that takes this dependence into account. Therefore, a MLM is applied as opposed to two individual models [*Mardia et al.*, 1979].

[21] The multivariate linear model used is $y_{\text{len}} = \mathbf{x}^T\boldsymbol{\beta}_{\text{len}} + \epsilon_{\text{len}}$ and $y_{\text{area}} = \mathbf{x}^T\boldsymbol{\beta}_{\text{area}} + \epsilon_{\text{area}}$, where $\mathbf{x}$ is a vector containing an intercept and the predictors, where $\boldsymbol{\beta}_{\text{len}}$ and $\boldsymbol{\beta}_{\text{area}}$ denote the coefficients, and where ϵ_{len} and ϵ_{area} are residual (jointly Gaussian) errors with mean zero, variances $\text{Var}(\epsilon_{\text{len}}) = \sigma_1^2$, $\text{Var}(\epsilon_{\text{area}}) = \sigma_2^2$ and correlation $\text{Cor}(\epsilon_{\text{len}}, \epsilon_{\text{area}}) = \rho$.

[22] Model space comprises 961 configurations, and model fitting is done with a likelihood approach, i.e., maximizing a bivariate Gaussian density over $\boldsymbol{\beta}_{\text{len}}$ and $\boldsymbol{\beta}_{\text{area}}$, σ_1^2, σ_2^2, and ρ, programmed with the software environment R [*Ihaka and Gentleman*, 1996; *R Development Core Team*, 2011]. Over-fitting is avoided through the use of a Bayesian Information Criterion (BIC). Figure 3 shows the 100 best models and the predictors chosen therein (cf. also Table S1, Figure S3 in the supporting information. We select the model with minimal BIC as the optimal one, which leads to the model

$$\widehat{y}_{\text{len}} = \widehat{\beta}_{\text{len},0} + \widehat{\beta}_{\text{len,ground}}x_{\text{ground}} + \widehat{\beta}_{\text{len,rise}}x_{\text{rise}} + \widehat{\beta}_{\text{len,geom}}x_{\text{geom}} + \widehat{\beta}_{\text{len,temp}}x_{\text{temp}}, \quad (1)$$

$$\widehat{y}_{\text{area}} = \widehat{\beta}_{\text{area},0} + \widehat{\beta}_{\text{area,ground}}x_{\text{ground}} + \widehat{\beta}_{\text{area,geom}}x_{\text{geom}}, \quad (2)$$

where a hat indicates an estimated quantity. Ice thickness at the grounding line, x_{thick}, does not enter the optimal model. Further, the correlation in the errors (estimate of 0.33) is not significant (likelihood ratio test yields a p-value of 0.19). Table 4 lists the estimated coefficients of the chosen, i.e., optimal, model along with their standard error. The choice of the optimal model is not clear cut, but the parameter estimates of the next best models are surprisingly stable. There is no indication of outliers or strong leverage effects in the data. For a more detailed mathematical description of the MLM, as well as a documentation of its predictive skill (cf. the supporting information, Appendices SC1 and SC2, and Figures S4 and S5).

2.3. Extreme Value Theory (EVT)

[23] In the following, we provide a description of how extreme drafts are statistically modeled. Sections 2.3.1

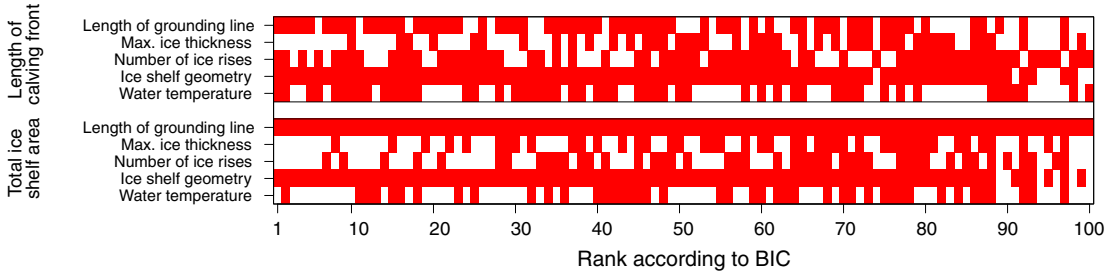

Figure 3. The 100 best models (in terms of BIC out of 961) obtained from the MLM. On the vertical axis, the responses y_{len} ("length of calving front") and y_{area} ("total ice shelf area") are shown, together with a list of all possible predictors. Red (white) boxes indicate that the predictor is (is not) contained in the model. On the horizontal axis, the 100 best models are listed, starting with the best model to the left. For the optimal model, y_{len} is given through all predictors except maximal ice thickness at the grounding line x_{thick}, while y_{area} depends on length of grounding line x_{len} and ice shelf geometry x_{geom} only. Note the dominance of certain predictors: e.g., x_{ground} is contained in all 100 best models for response y_{area}. Similarly, x_{geom} enters both y_{len} and y_{area} for the best 73 models.

and 2.3.2 give the theoretical background and detailed statistical justification for, among others, the methodology, threshold selection, chosen densities, etc. In addition, the following paragraph offers also a more intuitive description, facilitated by Figure 4 with data from the Drygalski ice tongue, capturing the essentials of the methodology in a nutshell accessible to a general audience.

[24] Starting from the raw draft data, evident outliers are identified (Figure 4a) and cleaned data are retained. We are interested in modeling the large drafts: thus, fitting a distribution to all draft values will not adequately address the problem as clearly shown by the histogram in Figure 4b. To restrict the analysis to large drafts, we select a threshold determining these (Figure 4b). Due to the relatively smooth draft, we have to thin the correlated data by identifying clusters and retaining only the cluster maxima (Figure 4c). An appropriate density is then fitted to this subset of draft values (Figure 4d). The fit is validated by comparing theoretical and empirical quantiles (Figure 4e) and by possibly readjusting the threshold. From the parameter estimates, return drafts and their uncertainties can be calculated, as illustrated by Figure 4f.

2.3.1. Rationale and Mathematical Background

[25] When statistically modeling the maximum value of a series or the maximum values of several series, it is dangerous to fit distributions from first- and second-order quantities and then to extrapolate to (very) small or (very) large quantiles. Consider the following example. Consider independent, standardized Gaussian random variables $X_1, \ldots, X_n$. The probability that any X_i is larger than 4 is $P(X_i > 4) = 3.167 \times 10^{-5}$. However, the probability that out of the samples of sizes 10, 100, and 1000, the maximum that exceeds 4 is $P(\max(X_1, \ldots, X_{10}) > 4) = 0.0003$, $P(\max(X_1, \ldots, X_{100}) > 4) = 0.0032$, and $P(\max(X_1, \ldots, X_{1000}) > 4) = 0.0312$ and naturally strongly depends on the sample size.

[26] Further, extreme cases are often caused by different physical mechanisms or processes than those governing the bulk of the data, and one should, therefore, not draw inferences from a distribution fitted over the bulk of the data.

[27] EVT addresses this issue by modeling the largest observation(s) directly. Indeed, these extreme observations behave asymptotically differently than the central values (which are asymptotically—under suitable conditions—from a normal distribution): it can be shown that for a large class of distributions F, the distribution of the (normalized) maximum $\max_i X_i$, where $X_1, \ldots, X_n$ are independent, identically distributed random variables according to F, converges to the so-called generalized extreme value distribution (GEVD) parameterized by a location μ, scale $\tilde{\sigma}$, and a shape parameter ξ [Fisher-Tippett Theorem; *Coles*, 2001, Thm 3.1.1; *Embrechts et al.*, 1997, Theorem 3.2.3]. The GEVD can also be characterized by the cases $\xi < 0$, $\xi = 0$, and $\xi > 0$.

[28] Note that the conditions on the distribution F that guarantee convergence to the GEVD are mathematically quite involved and are therefore not detailed here. For example, in the case of $\xi > 0$, one needs to establish that $1 - F(x) \sim x^{-\alpha} L(x)$, $\alpha > 0$ for some slowly varying function L [*Embrechts et al.*, 1997, Thm. 3.3.7]. However, virtually all of the classical distributions imply convergence, for example, Cauchy, Pareto, Loggamma ($\xi > 0$); Uniform, Beta ($\xi < 0$); Gamma, Normal, Lognormal ($\xi = 0$).

[29] Conceptually, EVT comprises three different approaches which are all interlinked. The first approach models only the maximum, the second approach models data exceeding a threshold (peak over threshold, POT), and the third one uses a Poisson process model for POTs. All

Table 4. Parameter Estimates of the Regression Analysis Along With the Adjusted Coefficient of Determination R^2_{adj} (With Standard Errors in Parenthesis) For the Optimal Model [a]

	Length of Calving Front, y_{len}	Total Ice Shelf Area, y_{area}
β_0	1.93 (0.98)	–0.33 (0.53)
β_{ground}	0.37 (0.17)	1.60 (0.08)
β_{thick}	-	-
β_{rise}	0.12 (0.06)	-
β_{geom}	–1.25 (0.24)	–0.76 (0.17)
β_{temp}	–1.13 (0.45)	-
σ^2	0.39^2	0.33^2
R^2_{adj}	0.84	0.96

[a] β_0 is the intercept, β_{ground} the coefficient of x_{ground} (log scale), β_{rise} the coefficient of x_{rise}, etc. Hyphen indicates that the predictor is not in the optimal model.

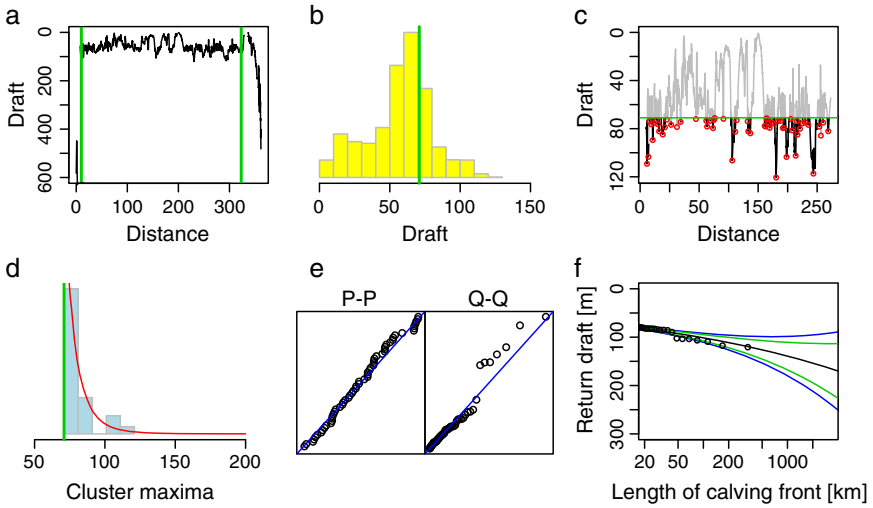

Figure 4. POT approach exemplified for Drygalski ice tongue. (a) Raw draft values are cleaned (stretches between green vertical bars). (b) A large threshold value is selected and (c) the data is declustered to yield cluster maxima (red dots). (d) Using these maxima, the GPD is fitted. Threshold selection is validated (cf. also, e.g., Figure A7) and (iteratively) adjusted. (e) Validation of GPD fit by comparing theoretical and empirical quantiles. (f) From parameter estimates, return drafts and their uncertainties are constructed. A detailed description and plots for all other shelves are given in the supporting information.

three approaches are interlinked, but, depending on the situation, some may be more suitable than others. For further details, we refer to the accessible text of *Coles* [2001], as well as to the supporting information, Appendix SD.

2.3.2. Modeling Extreme Drafts Using EVT/POT

[30] Because iceberg plowmarks at the Arctic Ocean seafloor, mapped as deep as ∼1000 m below present sea level, indisputably represent examples of extreme ice-draft events, EVT/POT is the best-suited statistical modeling framework. Modeling extreme drafts using the POT approach begins with extracting, from the ICESat data, y_{draft} as a series of observations along the calving fronts of the 17 contemporary Antarctic ice shelves considered in the MLM.

[31] In a nutshell, let D be a random variable with distribution F. To look at extreme events, we describe the probability of D exceeding a large threshold value u by an additional amount $y > 0$. This conditional probability is

$$P(D-u>y|D>u)=\frac{1-F(u+y)}{1-F(u)},\quad y>0.$$

In practice, F is not known. However, under conditions not specified here [*Coles*, 2001], the distribution for $D-u$, given $D > u$, for large enough u, is

$$\begin{aligned} &P(D-u\le y|D>u)\approx 1-(1+(\xi y/\sigma))^{-1/\xi},\\ &y>0 \text{ and } 1+\xi y/\sigma>0,\quad \sigma=\tilde{\sigma}+\xi(u-\mu), \end{aligned} \tag{3}$$

and μ, $\tilde{\sigma}$, ξ as in the GEVD (cf. section 2.3.1). The approximation is to be understood as a limiting argument as u increases. The right hand side of equation (3) is termed the generalized Pareto distribution (GPD), which, due to the presence of ξ and σ (the shape and scale parameters, describing the distribution's tail and spread, respectively), represents a family of distributions. Note that the GPD does not explicitly depend on F.

[32] To quantify the occurrence of extreme events, we calculate quantiles of the exceedances (that is, values exceeding the threshold u), originally termed "return level" in the context of extreme floods. Mathematically, the calculation of these quantiles requires the derivation of $P(D-u>y)$ (cf. the supporting information, see Appendix SD2 for more details).

[33] In our specific application, the observations described by the random variable D above are the drafts along the calving front, y_{draft}. However, the draft data is not independently distributed: nearby values are alike as they fluctuate slower than their resolution (cf. Figure S6). As equation (3) is valid for independently distributed variables only, we run a declustering algorithm over the draft data. Essentially, this means that exceedances (values of y_{draft} which are larger than some preassigned threshold u) are assigned to the same cluster if they are separated by fewer than a specified number (called "run length") of values above the threshold u. Threshold selection is based on plots of parameter estimates against different thresholds, and we opted for a universal threshold of the 75th percentile of the draft using a run length of 2 for declustering (Figures SA8 and SA9). Declustering reduces the draft data considerably (for example, to 17 values for Ekström and 71 for the Ross ice shelf (Table S2)). Further, within each cluster, only the largest value is retained and those largest values are referred to as cluster maxima. The cluster maxima are assumed to be independent, and their probability distribution is assumed to converge to a GPD.

[34] We emphasize that the model is based on (statistically) typical assumptions that are required for reasons of mathematical rigor (for further details on the POT approach and especially on the threshold selection, cf. the supporting information, Appendix SD). Under these assumptions, a GPD is inherently the limiting distribution for increasing length of calving front, and thus, we have eliminated shelves with short, interrupted draft sequences (namely, Abbot ice shelf, Dotson ice shelf, Getz ice shelf, Ninnis Glacier, Pine Island Glacier, cf. Table 1).

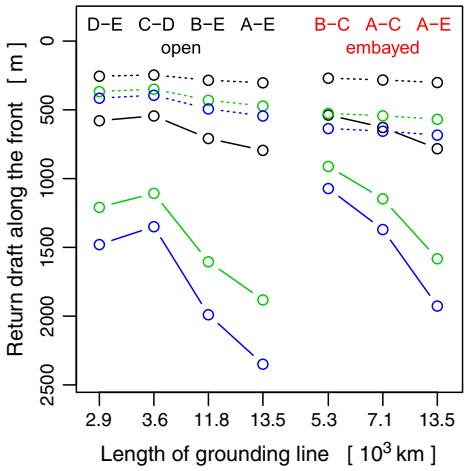

Figure 5. Return draft (black lines) along the calving front, for seven hypothetical Arctic Ocean paleo ice shelves, and as a function of grounding line length. Crude upper 75% (green) and 90% (blue) uncertainty bounds of the return level, constructed from Wald-type confidence intervals. The dotted lines (all colors) are based on median parameter estimates, while the solid lines (all colors) are based on the third quartile estimates. Water temperature is set to –1.8°C, the effect of different water temperatures is shown in Figure S11 in the supporting information.

[35] Finally, using the observed cluster maxima, we estimate the parameters ξ and σ of the GPD in equation (3) using maximum likelihood (Table S2), cf. also Figure 4d, which illustrates the fit of the GPD to the cluster maxima based on data for Drygalski ice tongue. These estimates are (naturally) sensitive to quantile and run length, but summary statistics based on the estimates from all shelves are very stable. The fitted distributions are assessed with probability-probability and quantile-quantile plots and match the data well (Figure S10). For some shelves, empirical quantiles are slightly higher than theoretical ones, indicating a conservative estimation of the tail heaviness. In our case, a heavier tail implies predictions of larger extreme calving front values, also reflected by the different choices of parameter estimates in section 3. Note that the parameters of the GPD are not expressed in terms of predictors, and thus, per se, no prediction is performed.

3. Results From Model Application in the Paleo-Arctic Setting

[36] We consider a Paleo-Arctic Ocean scenario and apply the fitted models from Antarctic data described in sections 2.2 and 2.3 in a setting where individual ice shelves form along the grounding line segments B–C, C–D, D–E, A–C, A–E, and B–E (Figure 1). In other words, for these segments, calving front length y_{len} and ice shelf area y_{area} are predicted based on the MLM, while maximal draft values and the return draft are estimated using EVT (and, importantly depend on estimates of y_{len} and thus on x_{ground}, x_{rise}, x_{geom}, and x_{temp}).

[37] The first result from model application in the paleo-Arctic setting is presented in Figure 5. There the return drafts of seven Arctic paleo ice shelves are shown, namely: for four ice shelf segments classified as open, and for three ice shelf segments classified as embayed. Segment A–E occurs twice to illustrate the impact of classification on the results. For each segment, return drafts are plotted with y_{len} set to the predicted mean from the MLM, and for a water temperature $x_{\text{temp}} = -1.8$°C along the calving front. Note that –1.8°C corresponds to the rounded 25th percentile of x_{temp} as used in our analysis, a value commonly employed for freezing of seawater (35 ppm) and sea ice formation in Ocean Circulation Modeling (cf. Figure S11 for return drafts at 0°C, –1°C, –2°C). With x_{temp} and y_{len} set (cf. Table 3), return drafts can be plotted as a function of grounding line length, x_{ground}. For all segments except B–C, drafts exceeding 910 m are within the 75% upper uncertainty bound if based on the third quartile estimates. If based on median parameter estimates, return drafts do not exceed 500 m even within the 75% upper uncertainty bound. Highest return drafts are obtained for segment A–E irrespective of its classification.

[38] Technically, predictions of the draft along paleo-Arctic ice shelf calving fronts as shown in Figure 5 are obtained as follows. The threshold as well as the GPD estimates and their uncertainties hardly correlate with the predictors used in the MLM. Hence, for the Paleo-Arctic setting, we only assume that similar parameter values are applicable. Thus, we first assume that the average draft threshold over all open/embayed ice shelves is a generic threshold for open/embayed ice shelves (Table S2). Second, we choose the following: (a) the median and (b) the third quartile of the estimates and the uncertainties for open/embayed shelves as shape (ξ) and scale (σ) parameters when applying the model in the paleo-Arctic setting (Table 5). Choices for ξ based on a quartile argument are justified, given the uncertainty in the estimates. For open shelves, the selected value is covered by all confidence intervals except for Mertz Glacier. Thus, the parameters yield a "predictive" distribution along with its quantiles for the return levels. Recall that a typical illustration of the concept of return level is a 100 year flood, for which the return level has 1% chance of being exceeded in a given year; the return period is 1/0.01 = 100 years [*Katz et al.*, 2002]. Here the return period is associated with the length of the calving front instead of time. Thus, the m-kilometer return draft $y_m + u$ is expected to be exceeded on average once every m kilometers along the calving front.

[39] The second result from model application in the paleo-Arctic setting is presented in Figure 6, where the joint

Table 5. Parameter Estimates (Threshold Draft Values u in Meters, Shape and Scale Parameters as Well as their Uncertainties) Used in the EVT Model Portation for the Two Different Ice Shelf Classes "Open" and "Embayed" [a]

	Open Shelf		Embayed Shelf	
	Median	3rd Quartile	Median	3rd Quartile
Threshold	92.24	92.24	159.73	159.73
Shape	0.17	0.38	0.03	0.50
Scale	26.53	38.83	33.20	43.31
Var(shape)	0.08	0.14	0.07	0.17
Var(scale)	54.60	243.43	90.38	171.38
Cov(shape,scale)	–1.66	–0.69	–1.71	–1.70

[a] Var(·) and Cov(·, ·) denote the variance and covariance, respectively.

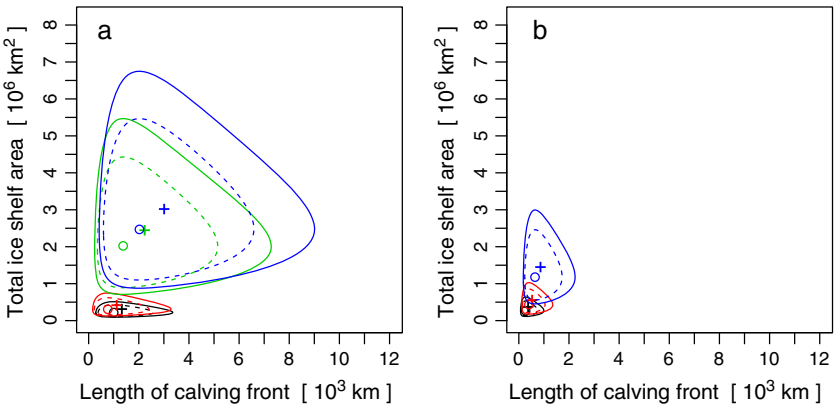

Figure 6. Joint predictive distribution of responses length of calving front, y_{len}, and total ice shelf area, y_{area} for seven hypothetical ice shelves forming along (combinations of) Arctic Ocean paleo-grounding line segments given a water temperature of –1.8°C (for segments cf. Figure 1). Solid (dotted) lines denote the 90% (75%) confidence regions, circles indicate the mode (highest density), and crosses the predicted mean responses of y_{len} and y_{area}. (a) Open ice shelves forming along segments A–E (blue lines and symbols), B–E (green lines and symbols), C–D (red lines and symbols), and D–E (black lines and symbols). (b) Embayed ice shelves forming along segments A–E (blue lines and symbols), A–C (red lines and symbols), and B–C (black lines and symbols). The asymmetry is a result of the back-transformation to the original scale. The corresponding results for water temperatures 0°C, –1°C, –2°C are shown in Figure S12 in the supporting information.

predictive distribution of the calving front length y_{len} and ice shelf area y_{area} is plotted for Arctic Ocean ice shelves forming along (combinations of) segments sketched in Figure 1. Results for open shelves (Figure 6a) and embayed shelves (Figure 6b) are displayed, with water temperature x_{temp} set to –1.8°C along all calving fronts (for 0°C, –1°C, –2°C, cf. Figure S12). Circles denote the mode (highest density, indicating the most likely configuration), crosses denote the predicted mean responses of y_{len} and y_{area}. The solid (dashed) curves encompass the 90% (75%) confidence regions of the joint prediction of y_{len} and y_{area}. Comparing Figures 6a and 6b, it is seen that in the paleo-Arctic setting, the predicted joint distribution of y_{len} and y_{area} has a wider range for open shelves than those for embayed ones. Further, the influence of the classification of ice shelf geometry is illustrated by performing predictions for segment A–E twice, treating it successively as open and embayed. In the particular case of segment A–E, the mean calving front length changes from $\sim$860 km (embayed) to $\sim$3010 km (open), while the associated ice shelf area changes from $\sim 1.4 \times 10^6$ km^2 (embayed) to $\sim 2.9 \times 10^6$ km^2 (open). It must be emphasized, however, that the predictive distributions do not incorporate any physical constraints, e.g., that for a particular length of the calving front the total area cannot exceed certain values (see section 4).

[40] Technically, the joint distributions are derived from equations (1) and (2) using the predictors given in Table 3, the estimated coefficients given in Table 4, and the prediction and estimation uncertainty again given in Table 4. The marginal predictive distribution of the log-response is a non-central Student's *t*-distribution. The joint predictive density of the responses (the product of the back-transformed marginal ones) is not spherically symmetric around its mode. The strong asymmetry in Figures 6 and S12 is induced by the back-transformation to the original scale: An increase of 1° in water temperature results in roughly one unit increase in the length of the calving front in the log scale (Table 2), implying the strong changes in the original scale. Yet predictions for 0°C have to be interpreted with caution as observed temperatures range between –1°C and –2°C.

4. Discussion

[41] The idea of reconstructing Arctic Ocean paleo ice sheets based on analogies with Antarctica is far from new. *Mercer* [1970] pointed out similarities between the Arctic Ocean and the ancient sea now taken over by the West Antarctic Ice Sheet's domes, ice streams, and ice shelves. Both areas are close to the geographic poles, and both are virtually landlocked. The West Antarctic Ice Sheet must be removed in order to envision that there once existed a partly landlocked sea there. From these observed analogies, *Mercer* [1970] suggested that similarly to West Antarctica, the Arctic Ocean during glacial periods hosted thick ice shelves, fed by ice streams draining large marine ice domes. Further building on Arctic-Antarctic analogies, *Hughes et al.* [1977] suggested that ice shelves must have filled the entire Arctic Ocean during the Last Glacial Maximum (LGM) in order to prevent the marine portions of the North American and Eurasian ice sheets from collapsing. Since the first mapping, data revealed traces of ice grounding in the central Arctic Ocean as deep as 1000 m below the present sea level [*Jakobsson*, 1999; *Polyak and Jakobsson*, 2011], the hypothesis of huge thick paleo ice shelves covering the Arctic Ocean has been revisited and discussed in numerous articles, e.g., [*Bradley and England*, 2008; *Engels et al.*, 2008; *Grosswald and Hughes*, 2008; *Jakobsson et al.*, 2010]. Studies of sediment cores suggest that the largest and deepest drafting ice shelves existed during Marine Isotope Stage 6, about 140,000 years ago, [*Jakobsson et al.*, 2010].

[42] Due to the situation that contemporary three-dimensional thermomechanical numerical ice models are

still challenged by the marginal ice dynamics in coupled sheet/stream/shelf complexes, we explored a statistical approach to address plausible extents of a MIS 6 Arctic Ocean ice shelf. We followed the line of thought suggested by *Mercer* [1970] and assumed that MIS 6 Arctic Ocean ice shelves behaved similarly to current Antarctic ice shelves, and that they also were scaled similarly. This assumption forms the basis for our statistical modeling approach. It is a strong assumption that naturally could be debated. However, we consider it a viable working hypothesis. It should be noted that not all Antarctic ice shelves were incorporated in our statistical "tuning" database. For instance, ice shelves with rather heterogeneous physiography have not been considered, as their classification is beyond the capabilities of the predictor x_{geom}. The simple geometric criterion on which the classification of an ice shelf as either open or embayed is based can not be applied to ice shelf configurations that are, e.g., pinned at their seaward edge, by a (chain of) islands/ice rises. Furthermore, it is of limited use in the classification of ice shelves that have joint boundaries with other ice shelves, such as, e.g., the Brunt ice shelf and the Riiser-Larsen ice shelf. For the 17 ice shelves considered here, x_{geom} proved a useful and stable predictor. Moreover, we consider it acceptable to disregard Antarctic Peninsula ice shelves from the analysis because it seems far-fetched to claim, in the spirit of *Mercer* [1970], similarities between their general configuration and possible Arctic Ocean paleo ice shelves.

[43] A yet unresolved issue in the analogy approach is that the largest Antarctic ice shelves presently generally do not produce icebergs drafting deeper than $\sim$350 m, while plowmarks in water depths deeper than 500 m are attributed to icebergs originating from either outlet glaciers or ice shelves fed from major interior basins [*Dowdeswell and Bamber*, 2007]. Plowmarks comparable in depth to the ones mapped in the Arctic Ocean have not yet been detected in the Antarctic.

[44] However, basal accretion is observed for a number of Antarctic ice shelves [*Zotikov et al.*, 1980; *Engelhardt and Determann*, 1987; *Oerter et al.*, 1992; *Khazendar et al.*, 2001] and has been suggested as a possible mechanism responsible for seaward thickening of ice shelves. In *Jakobsson et al.* [2010], it is hypothesized that Atlantic waters might not have entered the Amerasian Basin during glacial periods so that the Canada Basin might have become a very cold environment with great potential for accretion and, hence, deep-draft ice shelves.

[45] We note that modeled predictions of return draft for embayed ice shelves appear counter-intuitive at first sight, as they can be smaller than return draft for open shelves. However, this must be viewed against the fact that the draft data of four of the eight Antarctic ice shelves classified as embayed could not be used in the EVT. Enlarging the database by more draft data for contemporary Antarctic ice shelves of type embayed will likely yield improved predictions, but, as yet, awaits implementation.

[46] Improved predictions are also expected once spatially variable fields such as water temperature along the calving front, x_{temp}, are no longer reduced to a single number prior to entering the MLM. The crude averaging techniques applied in the derivation of x_{temp} render x_{temp} a less stable predictor than, e.g., grounding line length, x_{ground}, and ice shelf geometry, x_{geom} (cf. Figure 3). Once the variation of x_{temp} with latitude, longitude, and depth is accounted for in the MLM, we expect x_{temp} to play an increasingly important role as predictor in our statistical framework reflecting, eventually, observationally confirmed evidence [*Jenkins et al.*, 2010]. Until then, we refrain from considering additional spatially variable fields as predictors, although, e.g., surface air temperature data is available for all ice shelves.

[47] The three-step statistical approach proposed here results in reasonably simple and robust models. The results would remain essentially the same even if minor technical model refinements were made such as the use of a formal BIC criterion in the MLM in step 1, or employment of an automatic threshold selection in the POT/EVT context in step 2. Although the EVT modeling is performed for an ice shelf complex at one (arbitrary) point in time, we argue that considering "replicates" over time in order to produce a predictive distribution for the return draft will likely not lead to improved insights due to the uncertainties associated with the estimation of the return draft. However, it should be kept in mind that Antarctic ice shelves are currently at interglacial extents. Therefore, our predictions for Paleo-Arctic Ocean ice shelf configurations are likely to represent lower bounds for the glacial MIS 6 ice shelf complex.

[48] The main goal for our statistical modeling was to address whether the mapped traces of ice grounding in the central Arctic Ocean could be caused by icebergs originating from an Amerasian ice shelf, if assuming an environment similar to that of Antarctic ice shelves. The deepest mapped ice grounding is located on Morris Jesup Rise, and it exceeds the present water depth of 1000 m (Figure 1c). However, those iceberg plowmarks are from singular deep-drafting icebergs. It has been shown that icebergs occasionally capsize and, for a short duration of time, they reach depths greater than their original drafts. This cannot be excluded in the Morris Jesup Rise case. On the other hand, the scours on Chukchi Borderland, Yermak Plateau, and Lomonosov Ridge clearly suggest armadas of icebergs, likely composed of tabular icebergs originating from ice shelves [*Dowdeswell et al*., 2010; *Jakobsson et al*., 2010]. The features resembling mega-scale glacial lineations on Chukchi Borderland and Yermak Plateau are located in present water depths of $\sim$900 – 400 m and 530 m, respectively. It should be noted that the deepest ice grounding on the Lomonosov Ridge may have been caused by icebergs of Eurasian sources [*Jakobsson et al.*, 2008b; *Kristoffersen et al.*, 2004; *Polyak and Jakobsson*, 2011], although the presently available data are not conclusive.

[49] For all ice shelf segments considered, return drafts exceeding 910 m are not obtained when predictions are based on median estimates. However, based on third quartile estimates, return drafts exceeding 910 m lie within the 75% upper uncertainty bounds for all segments except B–C. We see this as a first indicator that the MIS 6 ice shelf complex must have comprised more than just an ice shelf along segment B–C, fed by ice streams in the Amundsen Gulf and McClure Strait only. Indeed, given a hypothetical extension of the ice shelf along B–C to the west (reaching the Chukchi Borderland, thus with grounding line A–C), predicted return drafts at the calving front larger than 910 m are within the 75% uncertainty bound. Similar return drafts are obtained for individual ice shelves along C–D, and D–E, respectively.

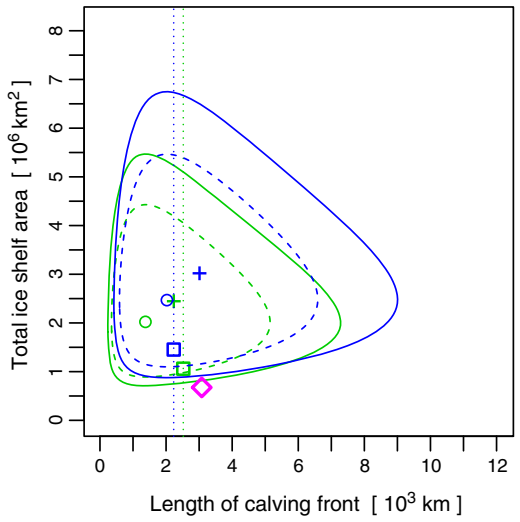

Figure 7. Joint predictive distribution of responses y_{len} and y_{area} for the hypothetical Arctic Ocean ice shelf complex forming along segments A–E (blue) and B–E (green) given a water temperature of –1.8° C (for segments cf. Figure 1). Solid (dashed) lines denote the 90% (75%) confidence regions, circles indicate the mode (highest density) and crosses the predicted mean responses of y_{len} and y_{area}. The dotted lines indicate the minimal calving length based on the geodetic distance on the sphere between the segment end points A–E and B–E, respectively. The associated ice shelf areas are marked by squares. The calving front length and area of the Arctic Ocean MIS 6 ice shelf complex suggested in *Jakobsson et al.* [2010] is marked by a magenta diamond.

These results suggest that a small, confined ice shelf in the Amerasian sector of the Arctic along B–C only can be excluded as a possible source of icebergs large enough to cause the plowmarks on the Morris Jesup Rise and the Yermak Plateau. Rather, such bergs could have calved from the fronts of an ice shelf complex extending either westward from McClure Strait and toward the Chukchi Borderland (A–C), or from east of McClure Strait to Ellesmere Island (C–D), or from Ellesmere Island to the northernmost coast of Greenland (fed by an ice stream in Nares Strait, segment C–D). Combining these ice shelves into one extending from Point Barrow to the northernmost coast of Greenland (B–E), return drafts of 780 m are modeled based on third quartile estimates. Within the 75% upper uncertainty bound, return drafts exceed 1500 m for segment B–E. Similar results are obtained if the ice shelf complex extends from the Chukchi Borderland (A–E). Since three independent and individual ice shelf configurations (A–C, C–D, and D–E) are modeled to have calving fronts allowing for return drafts exceeding ∼910 m within the 75% upper uncertainty bound, we argue that one should not, a priori, claim ice shelves to be absent from either one of those regions. Hence, our statistical analysis of the Arctic Ocean MIS 6 ice shelf complex proposed by *Jakobsson et al.* [2010] indicates that these large Amerasian Ocean ice shelves could indeed have been the sources of deep-draft icebergs, the traces of which have been mapped as deep as ∼1000 m below the present day sea level in parts of the central Arctic Ocean.

[50] As the MLM approach involves a crude classification of ice shelf geometry only, exact topographies of an Arctic MIS 6 ice shelf configuration can not be modeled. For example, consider the shelves with grounding line A–E and B–E. The former has a larger grounding line and the prediction of y_{len}, y_{area} are thus larger compared with the latter. However, the minimal calving length based on the geodetic distance of the segment end points on the sphere are 2231 km (A–E) and 2521 km (B–E), indicated by the dotted lines in Figure 7. The associated ice shelf areas are measured as 1.45×10^6 km^2 (A–E) and 1.06×10^6 km^2 (B–E), and are marked by squares in Figure 7. The magenta diamond indicates length of calving front (3080 km) and ice shelf area (675,801 km^2) for the MIS 6 ice shelf complex proposed by *Jakobsson et al.* [2010]. According to the statistical model proposed here, this ice shelf configuration is just outside the 90% confidence region (configuration B–E). This may indicate that either *Jakobsson et al.* [2010] slightly underestimated the ice shelf extent or that modeled ice shelf areas are overestimated when applying the model in the paleo-Arctic setting.

5. Conclusions

[51] Spatial reconstructions of Quaternary glaciations in the Arctic Ocean region portray multiple episodes of glacial advances and retreats, associated with repetitive impact from floating ice shelves fringing the waxing and waning continental Amerasian and Eurasian ice sheets [*Dyke et al.*, 2002; *Svendsen et al.*, 2004; *Jakobsson et al.*, 2010]. Marine glacigenic landforms used to reconstruct Quaternary glacial conditions in the Arctic Ocean include mega-scale glacial lineations, iceberg plowmarks, flutes, and redeposited sediment accumulations [*Jakobsson et al.*, 2008b; *O'Regan et al.*, 2010]. The remarkable depths—approximately 1000 m below the present sea level—at which iceberg deep-draft scours are mapped in the Arctic Ocean, call for a modeling approach designed to complement the available observational evidence, and eventually, the spatial reconstructions based on geophysical mapping alone.

[52] We have proposed a statistical model in which the general dimensions of Arctic Ocean paleo ice shelves are predicted from relations between contemporary Antarctic ice shelf dimensions and their local physical environments. Critical to the identification of possible sources of deep-drafting icebergs is a rigorous analysis of the ice shelves calving fronts' thicknesses. We have employed extreme value theory to account for the fact that the mapped deep-draft plowmarks must rather be extreme events than common ones. Thereby, our model predictions of extreme drafts for an Arctic Ocean paleo ice shelf complex are derived within a firmly based statistical framework that is specifically designed to deal with extreme, rather than common events. Indeed, predicted extreme ice shelf drafts match observed deep-draft iceberg scours if the ice shelf complex is sufficiently large. Thus, additional modeling based support is provided in favor of the extensive MIS 6 ice shelf complex discussed by *Jakobsson et al.* [2010], and which hitherto was inferred from interpretation of geophysical and geological data only.

[53] The three-step statistical model proposed here is robust, however, further refinements are possible. Obviously, considering more ice shelves and more data in the

MLM is one option. However, a better representation of variables that have until now entered the MLM in a very simplified manner (water temperature) will likely yield more substantial improvements than those achievable by simply increasing the amount of data. Only after spatially variable fields can be properly accounted for is it reasonable to include, e.g., surface air temperature and sub-ice shelf melt/accretion rates.

[54] Furthermore, the statistical approach itself can also be refined. Instead of the static approach chosen here, a hierarchical dynamical spatio-temporal statistical model could be employed. Then, the draft (or, more generally, ice shelf thickness over time) is stochastically modeled using input variables like ice thickness at and ice flux across the grounding line, ice flow velocity, water temperature, etc. Such a stochastic model would consist of simplified dynamic partial differential equations governing ice shelf dynamics complemented with (prior) distributions for all unknown parameters or unresolved processes, and would, as such, be able to shed light on especially the temporal evolution of Arctic Ocean paleo ice shelf complexes.

[55] **Acknowledgments.** N.K. and R.F. are joint first authors of this manuscript. N.K. thanks C. Stover Wiederwohl, Texas A&M University, for introduction to and guidance through the WOCE-SODB database during the "Oden Southern Ocean 0910" cruise to Pine Island Bay/West Antarctica. R.F. acknowledges funding from SNSF 129782, 143282 and URPP Systems Biology. This is a contribution from the Bolin Center for Climate Research at Stockholm University, Sweden. We thank the editor, Bryn Hubbard, the associate editor, Mike Bentley, as well as Jesse Johnson, and five anonymous reviewers for valuable comments on the manuscript.

References

Alvarez-Solas, J., M. Montoya, C. Ritz, G. Ramstein, S. Charbit, C. Dumas, K. Nisancioglu, T. Dokken, and A. Ganopolski (2011), Heinrich event 1: An example of dynamical ice-sheet reaction to oceanic changes, *Clim. Past*, *7*, 1297–1306, doi:10.5194/cp-7-1297-2011.

Bohlander, J., and T. Scambos (2007), *Antarctic Coastlines and Grounding Line Derived from MODIS Mosaic of Antarctica (MOA)*, National Snow and Ice Data Center. Digital media, Boulder, Colorado USA .

Bradley, R. S., and J. H. England (2008), The Younger Dryas and the sea of ancient ice, *Quaternary Res.*, *70*(1), 1–10, doi:10.1016/j.yqres.2008.03.002.

Broecker, W. (1975), Floating glacial ice caps in the Artic Ocean, *Science*, *188*, 1116–1118.

Coles, S. (2001), *An Introduction to Statistical Modeling of Extreme Values*, 208 p., Springer, New York.

DeConto, R., D. Pollard, and D. Harwood (2007), Sea ice feedback and Cenozoic evolution of Antarctic climate and ice sheets, *Paleoceanography*, *22*, PA3214, doi:10.1029/2006PA001350.

DiMarzio, J., A. Brenner, R. Schutz, C. A. Shuman, and H. J. Zwally (2007), *GLAS/ICESat 500 m Laser Altimetry Digital Elevation Model of Antarctica*, National Snow and Ice Data Center. Digital media, Boulder, Colorado USA.

Dowdeswell, J. A., and J. L. Bamber (2007), Keel depths of modern Antarctic icebergs and implications for sea-floor scouring in the geological record, *Mar. Geol.*, *243*(1–4), 120–131, doi:10.1016/j.margeo.2007.04.008.

Dowdeswell, J. A., et al. (2010), High-resolution geophysical observations from the Yermak Plateau and northern Svalbard margin: Implications for ice-sheet grounding and deep-keeled icebergs, *Quat. Sci. Rev.*, *29*, 3518–3531, doi:10.1016/j.quascirev.2010.06.002.

Dyke, A. S., J. T. Andrews, P. U. Clark, J. H. England, G. H. Miller, J. Shaw, and J. J. Veillette (2002), The Laurentide and Innuitian ice sheets during the last glacial maximum, *Quat. Sci. Rev.*, *21*, 9–31.

Embrechts, P, C. Klüppelberg, and T. Mikosch (1997), *Modelling Extremal Events for Insurance and Finance*, 645 pages, Springer, Berlin.

Engelhardt, H., and J. Determann (1987), Borehole evidence for a thick layer of basal ice in the central Ronne Ice Shelf, *Nature*, *327*(6120), 318–319, doi:10.1038/327318a0.

Engels, J. L., M. H. Edwards, L. Polyak, and P. D. Johnson (2008), Seafloor evidence for ice shelf flow across the Alaska-Beaufort margin of the Arctic Ocean, *Earth Surf. Proc. Land*, *32*, 1–17, doi:10.1002/esp.1601.

England, J. H., M. F. A. Furze, and J. P. Doupe (2009), Revision of the NW Laurentide Ice Sheet: Implications for paleoclimate, the northeast extremity of Beringia, and Arctic Ocean sedimentation, *Quaternary Sci. Rev.*, *28*, 1573–1596, doi:10.1016/j.quascirev.2009.04.

Ewing, M., and W. L. Donn (1956), A theory of ice ages, *Science*, *123*, 1061–1066.

Fyke, J. G., A. J. Weaver, D. Pollard, M. Eby, L. Carter, and A. Mackintosh (2011), A new coupled ice sheet/climate model: Description and sensitivity to model physics under Eemian, Last Glacial Maximum, late Holocene and modern climate conditions, *Geosci. Model Dev.*, *4*, 117–136, doi:10.5194/qmd-4-117-2011.

Grosswald, M. G., and T. J. Hughes (2008), The case for an ice shelf in the Pleistocene Arctic Ocean, *Polar Geograp.*, *31*, 69–68, doi:http://dx.doi.org/10.1080/10880370802175929.

Hindmarsh, R. A. C. (2009), Consistent generation of ice-streams via thermo-viscous instabilities modulated by membrane stresses, *Geophys. Res. Lett.*, *36*, L06502, doi:10.1029/2008GL036877.

Hughes, T. J., G. H. Denton, and M. G. Grosswald (1977), Was there a late-Würm Arctic ice sheet? *Nature*, *266*, 596–602.

Ihaka, R., and R. Gentleman (1996), R: A language for data analysis and graphics, *J. Comput. Graph. Stat.*, *5*, 299–314.

Jakobsson, M. (1999), First high-resolution chirp sonar profiles from the central Arctic Ocean reveal erosion of Lomonsov Ridge sediments, *Mar. Geol.*, *158*, 111–123.

Jakobsson, M., R. Macnab, L. Mayer, R. Anderson, M. Edwards, J. Hatzky, H. W. Schenke, and P. Johnson (2008a), An improved bathymetric portrayal of the Arctic Ocean: Implications for ocean modeling and geological, geophysical and oceanographic analyses, *Geophys. Res. Lett.*, *35*, L07602, doi:10.1029/2008GL033520.

Jakobsson, M., L. Polyak, M. Edwards, J. Kleman, and B. Coakley (2008b), Glacial geomorphology of the Central Arctic Ocean: The Chukchi Borderland and the Lomonosov Ridge, *Earth Surf. Proc. Land.*, *33*, 526–545, doi:10.1029/2008GL033520.

Jakobsson, M., et al. (2010), An Arctic Ocean ice shelf during MIS 6 constrained by new geophysical and geological data, *Quat. Sci. Rev.*, *29*, 3505–3517, doi:10.1016/j.quascirev.2010.03.015.

Jenkins, A., P. Dutrieux, S. S. Jacobs, S. D. McPhail, J. R. Perrett, A. T. Webb, and D. White (2010), Observations beneath Pine Island Glacier in West Antarctica and implications for its retreat, *Nat. Geosci.*, *3*, 468–472, doi:10.1038/ngeo890.

Katz, R. W., M. B. Parlange, and P. Naveau (2002), Statistics of extremes in hydrology, *Adv. Water Resour.*, *25*, 1287–1304.

Khazendar, A., J. L. Tison, B. Stenni, M. Dini, and A. Bondesan (2001), Significant marine-ice accumulation in the ablation zone beneath an Antarctic ice shelf, *J. Glaciol.*, *47*(158), 359–368, doi:org/10.3189/172756501781832160.

Kirchner, N., K. Hutter, M. Jakobsson, and R. Gyllencreutz (2011), Capabilities and limitations of numerical ice sheet models: A discussion for earth scientists and modelers, *Quat. Sci. Rev.*, *30*, 3691–3704, doi:10.1016/j.quascirev.2011.09.012.

Kleman, J., C. Hättestrand, A. Stroeven, and I. Borgström (2006), Reconstruction of paleo-ice sheets - inversion of their glacial geomorphological record, in *Glaciology and Earth's Changing Environment*, edited by P. G. Knight, pp. 192–198, Blackwell Publishing Ltd., Oxford.

Kristoffersen, Y., B. Coakley, W. Jokat, M. Edwards, H. Brekke, and J. Gjengedal (2004), Seabed erosion on the Lomonosov Ridge, central Arctic Ocean: A tale of deep draft icebergs in the Eurasian Basin and the influence of Atlantic water inflow on iceberg motion? *Paleoceanography*, *19*, PA3006.

Mardia, K. V., J. T. Kent, and J. M. Bibby (1979), *Multivariate Analysis*, pp. 521, Academic Press , San Diego.

Mercer, J. H. (1970), A former ice sheet in the Arctic Ocean? *Paleogeo. Paleoclimatol. Paleoecol.*, *8*, 19–27.

Oerter, H., J. Kipfstuhl, J. Determann, H. Miller, D. Wagenbach, A. Minikin, and W. Graf (1992), Evidence for basal marine ice in the Filchner–Ronne Ice Shelf, *Nature*, *358*(6385), 399–401.

O'Regan, M., M. Jakobsson, and N. Kirchner (2010), Glacial geological implications of overconsolidated sediments on the Lomonosov Ridge and Yermak Plateau, *Quat. Sci. Rev.*, *29*, 3532–3544, doi:http://dx.doi.org/10.1016/j.quascirev.2010.09.009.

Orsi, A. H., and T. Whitworth III (2004), Hydrographic Atlas of the World Ocean Circulation Experiment (WOCE), in *Volume 1: Southern Ocean International WOCE Project Office*, edited by M. Sparrow, P. Chapman, and J. Gould, International WOCE Project Office, Southampton, U.K. ISBN 0-904175-49-9, http://wocesoatlas.tamu.edu.

Pattyn, F. (2003), A new three-dimensional higher-order thermomechanical ice sheet model: Basic sensitivity, ice stream development, and ice flow across subglacial lakes, *J Geophys. Res.*, *108*(B8), 2382, doi:10.1029/2002JB002329.

Peyaud, V., C. Ritz, and G. Krinner (2007), Modelling the Early Weichselian Eurasian Ice Sheets: Role of ice shelves and influence of ice-dammed lakes, *Clim. Past*, *3*, 375–386., http://www.clim-past.net/3/375/2007/.

Pollard, D., and R. M. DeConto (2009), Modelling West Antarctic ice sheet growth and collapse through the past five million years, *Nature*, *458*, 329–32, doi:10.1038/nature07809.

Polyak, L., M. H. Edwards, B. J. Coakley, and M. Jakobsson (2001), Ice shelves in the Pleistocene Arctic Ocean inferred from glaciogenic deep-sea bedforms, *Nature*, *410*, 453–457 (22 March 2001), doi:10.1038/35068536.

Polyak, L., and M. Jakobsson (2011), Quaternary sedimentation in the Arctic Ocean: Recent advances and further challenges, *Oceanography*, *24*(3), 52–64, doi:http://dx.doi.org/10.5670/oceanog.2011.55.

Rabineau, M., S. Berne, J.-L. Olivet, D. Aslanian, F. Guillocheau, and P. Joseph (2006), Paleo sea levels reconsidered from direct observation of paleoshoreline position during Glacial Maxima (for the last 500,000 yrs), *Earth Planet. Sci. Lett.*, *252*, 119–137, doi:10.1016/j.epsl.2006.09.033.

R Development Core Team (2011), R: A language and environment for statistical computing. R Foundation for Statistical Computing, Vienna, Austria. ISBN 3-900051-07-0, http://www.R-project.org.

Siegert, M., and J. A. Dowdeswell (1999), Late Weichselian glaciation of the Russian High Arctic, *Quat. Res.*, *52*, 273–285.

Siegert, M., J. A. Dowdeswell, M. Hald, and J. I. Svendsen (2001), Modeling the Eurasian Ice Sheet through a full (Weichselian) glacial cycle, *Global Planet. Change*, *31*, 367–385, doi:qres.1999.2082.

Svendsen, J. I., et al. (2004), Late Quaternary ice sheet history of northern Eurasia, *Quat. Sci. Rev.*, *23*, 1229–1271, doi:10.1126/science.207.4438.1463.

van der Veen, K., and ISMASS members, (2007), A need for more realistic ice sheet models. International Council for Science, Scientific Comittee on Antarctic Research (SCAR) Report 30.

Zotikov, I. A., V. S. Zagorodnov, and J. V. Raikovsky (1980), Core drilling throuh the Ross Ice Shelf (Antarctica) confirmed basal freezing, *Science*, *207*, 1463–1464, doi:10.1126/science.207.4438.1463.

Zwally, H. J., M. B. Giovinetto, J. Li, H. G. Cornejo, M. A. Beckley, A. C. Brenner, J. L. Saba, and D. Yi (2005), Mass changes of the Greenland and Antarctic ice sheets and shelves and contributions to sea-level rise: 1992–2002, *J. Glaciology*, *51*, 509–527.